



Accretion-driven Sources in Spatially Resolved Ly α Emitters

Benjamin Dittenber¹, M. S. Oey¹ , Edmund Hodges-Kluck^{2,3} , Elena Gallo¹, Matthew Hayes⁴ , Göran Östlin⁴, and Jens Melinder⁴ 

¹ University of Michigan, Department of Astronomy, Ann Arbor, MI 48109, USA

² University of Maryland, Department of Astronomy, College Park, MD 20742, USA

³ X-ray Laboratory, NASA Goddard Space Flight Center, Code 662, Greenbelt, MD 20770, USA

⁴ Stockholm University, Department of Astronomy and Oskar Klein Centre for Cosmoparticle Physics, AlbaNova University Centre, SE-10691 Stockholm, Sweden

Received 2019 December 11; revised 2020 January 31; accepted 2020 February 2; published 2020 February 13

Abstract

Ly α emission is a standard tracer of starburst galaxies at high redshift. However, a number of local Ly α emitters (LAEs) are X-ray sources, suggesting a possible origin of Ly α photons other than young, hot stars, and which may be active at much later ages relative to the parent starburst. Resolved, nearby LAEs offer the opportunity to discriminate between diffuse X-ray emission arising from supernova-heated gas, high-mass X-ray binaries (HMXBs), or low-luminosity active galactic nuclei (LLAGN). We examine archival X-ray imaging from *Chandra* and *XMM-Newton* for 11 galaxies with spatially resolved Ly α imaging to determine the luminosity, morphology, and spectral hardness of the X-ray sources. The data are consistent with 9 of the 12, bright Ly α sources being driven by luminous, $>10^{40}$ erg s $^{-1}$ X-ray sources. Half of the eight *Chandra* sources are unresolved. The data suggest that nuclear activity, whether from LLAGN or nuclear starbursts, may play an important role in Ly α emission. Our results also suggest a significant link between Ly α emission and HMXBs, ultraluminous X-ray sources, and/or LLAGN, which would imply that Ly α may be generated over timescales 1–2 orders of magnitude longer than produced by photoionization from OB stars. This highlights a critical need to quantify the relative contributions of different sources across cosmic time, to interpret Ly α observations and the resulting properties of distant galaxies.

Unified Astronomy Thesaurus concepts: Compact radiation sources (2899); Ultraviolet sources (1741); Extragalactic astronomy (506); High energy astrophysics (739); Starburst galaxies (1570); Emission line galaxies (459); Lyman-alpha galaxies (978); Low-luminosity active galactic nuclei (2033); X-ray active galactic nuclei (2035)

1. Introduction

Studies of galaxies at high redshift often rely on Ly α emission, which is produced in the recombination of ionized hydrogen and predicted to be associated with young massive stellar populations. More than five decades ago, Ly α was put forth as a tool to study high-redshift, star-forming galaxies due to its high luminosity and accessibility from Earth-based observatories (Partridge & Peebles 1967). Over the years, it has been used to probe the epoch of reionization (e.g., Malhotra & Rhoads 2004; Kashikawa et al. 2006; Stark et al. 2017), and numerous high-redshift galaxies have been discovered by narrowband Ly α imaging (e.g., Hu & McMahon 1996; Mallery et al. 2012) and integral field unit observations (e.g., Hashimoto et al. 2017; Herenz et al. 2019).

The complexity of Ly α radiative transfer complicates our interpretation of the conditions allowing its escape from the local environment. Since Ly α is a resonant transition, it scatters both spatially and spectrally. In addition, Ly α emission cannot be spatially resolved at high redshift, and therefore the contributing sources cannot be clearly determined. Thus, often only global measurements of total Ly α emission from distant galaxies are possible. These factors limit our understanding of the underlying astrophysical processes that generate Ly α emitters (LAEs) and subsequent interpretation of high-redshift observations.

Ly α emission is usually produced by photoionization, which in high-redshift, starburst galaxies is often assumed to originate from star-forming H II regions. However, accreting compact objects also produce ultraviolet ionizing photons, which

therefore are also a potential source of Ly α emission; for example, active galactic nuclei (AGN) are well-known LAEs (e.g., Calhau et al. 2020). These alternative sources are important because high-mass X-ray binaries (HMXBs) may considerably extend the period of Ly α emission from starbursts, since HMXBs form after the most massive stars have expired, and nuclear starbursts may also trigger accretion onto nuclear, massive black holes, which can be sustained at a low level for times on order 10^8 yr or more.

Local, spatially resolved LAEs can help clarify the origin of Ly α emission in starburst galaxies. Studying LAEs in X-rays can show whether most starburst LAEs are indeed generated by the photoionization from massive stars rather than AGN. For example, the starburst interacting galaxy system Haro 11 is an LAE with a bright, hard, compact X-ray source coinciding with the galaxy's only strong Ly α source. This X-ray emission appears to be due to an ultraluminous X-ray source (ULX; Prestwich et al. 2015). Sources like this cannot be attributed to shock-heated, diffuse gas from massive-star feedback, and they are more likely due to X-ray binaries (HMXBs) or low-luminosity active galactic nuclei (LLAGN; Prestwich et al. 2015; Oskinova et al. 2019).

In this work, we examine the X-ray emission from local starburst galaxies with confirmed, resolved Ly α imaging, and that also have archive X-ray data (e.g., Basu-Zych et al. 2013; Brorby et al. 2016) available. From these data we can determine whether HMXBs and/or LLAGN play a significant role in powering LAEs and/or facilitating Ly α escape. If HMXBs are responsible for LAEs, then Ly α may be still be

Table 1
X-Ray Observations

| Galaxy | Alt. ID | R.A. (J2000) | Decl. (J2000) | Observatory | ObsID | Exposure (ks) |
|-----------------|---------------------------|-----------------|------------------|-------------------|------------|------------------|
| Haro 11 | ESO 350-IG038 | 00:36:52.70 | -33:33:17.0 | <i>Chandra</i> | 16695 | 24.74 |
| NGC 6090 | Mrk 496 | 16:11:40.70 | +52:27:24.0 | <i>Chandra</i> | 6859 | 14.79 |
| IRAS 08339+6517 | | 08:38:23.18 | +65:07:15.2 | <i>XMM-Newton</i> | 0111400101 | 57.65 |
| ESO 338-IG004 | Tol 1924-416 | 19:27:58.17 | -41:34:32.2 | <i>XMM-Newton</i> | 0780790201 | 24 |
| LARS 01 | | 13:28:44.05 | +43:55:50.5 | <i>Chandra</i> | 19442 | 33.41 |
| LARS 03 | UGC 08335 | 13:15:34.98 | +62:07:28.7 | <i>Chandra</i> | 7810 | 14.85 |
| LARS 07 | Ton 151 | 13:16:03.92 | +29:22:54.1 | <i>XMM-Newton</i> | 0780790401 | 22 |
| LARS 08 | WISEA J125013.82+073444.7 | 12:50:13.85 | +07:34:44.5 | <i>XMM-Newton</i> | 0780790101 | 20 |
| LARS 09 | KUG 0820+282 | 08:23:54.95 | +28:06:21.6 | <i>Chandra</i> | 13012 | 8.89 |
| LARS 10 | Mrk 61 | 13:01:41.53 | +29:22:52.9 | <i>Chandra</i> | 15065 | 14.87 |
| LARS 12 | SBS 0934+546 | 09:38:13.50 | +54:28:25.1 | <i>Chandra</i> | 16018 | 15.47 |

linked to massive stellar clusters, but at a more evolved stage than photoionization by stellar radiation itself. This would imply that Ly α emission from starbursts is longer lived than when assumed to originate from only stellar photoionization.

2. Sample and Data Analysis

We use the local sample of starburst galaxies from Östlin et al. (2009) and the Lyman Alpha Reference Sample (LARS; Östlin et al. 2014), which are good analogs to high-redshift LAEs. These two samples target galaxies that are at distances of roughly 40 to 250 Mpc, and all have uniform, spatially resolved, Ly α imaging from the *Hubble Space Telescope*. The LARS objects were selected to omit targets with any nebular evidence of AGN (Östlin et al. 2014). In particular, the line width of H α must have FWHM $< 300 \text{ km s}^{-1}$, and second, the galaxies have H II-region-like, optical emission-line ratios.

From these samples, we select the objects that are confirmed LAEs and also have publicly available archival X-ray data from the *Chandra X-ray Observatory* ACIS-S and *XMM-Newton* EPIC-pn and MOS instruments. This yields 11 galaxies, given in Table 1, and shown in three-color images in Figures 1 and 2.

We followed standard analysis procedures, which for *Chandra* involved using the CIAO v4.9 software package. We used the `chandra_repro` script to create level = 2 event files and `deflare` to remove periods of high background flaring, excluding periods where the chip count rate exceeds the average by more than 3σ . We identified sources using the `wavdetect` tool with default detection thresholds on the 0.3–10 keV band, then calibrated the astrometry by cross-matching at least three detected sources with the Sloan Digital Sky Survey catalog or the USNO B1.0 catalog. We obtained the X-ray fluxes with the CIAO `srcflux` tool, using the “Ideal PSF” method for a circular aperture encompassing the entire galaxy’s emission, centered on the source, and using a source-free local background annulus. While this represents the integrated emission from all sources, there was one dominant source in each galaxy, except for the merging components of Haro 11 and NGC 6090, which were treated as individual galaxies. For the model flux, we assumed an absorbed power-law spectrum with a photon index $\Gamma = 2.0$ and with Galactic absorption based on the `coldden` tool. We caution that Γ has some variation for HMXBs and LLAGN (e.g., Terashima et al. 2002; Sazonov & Khabibullin 2017). For $\Gamma = (1.5, 2.5)$, the resulting flux is (0.8, 3) times the value obtained for $\Gamma = 2.0$. For any objects dominated by soft sources having larger values of Γ , the flux could be further underestimated.

For *XMM* data, we followed a similar procedure, using the SAS v17.0.0 software, and using the `epchain` and `emchain` scripts to calibrate the data and produce level = 2 event files. We filtered on the background light curve in the same way as for the *Chandra* data, and then detected sources and measured fluxes using the `edetect_chain` script. We set the image `binsize` to 22, corresponding to a resolution of $1''1$, and processed the separate images for 0.5–8.0 keV. EPIC-pn versus EPIC-MOS observations were chosen based on signal-to-noise ratio. The 90% confidence X-ray fluxes are given in Table 2.

3. X-Rays from Ly α Emitters

We find that in nearly every galaxy, there is X-ray emission consistent with the location of the Ly α emission identified by Hayes et al. (2014) and Östlin et al. (2009). One exception is LARS 09, which has a nuclear X-ray source while the Ly α source is at large galactocentric radius. Also, Haro 11 has two strong ULXs, while only one is a strong LAE (Prestwich et al. 2015); and NGC 6090 is a major merger with Ly α and X-ray emission from both the NE and SW components. The component sources in these mergers are listed separately in Table 2.

3.1. Angular Sizes

We can use the angular size of the source to constrain the origin of the X-ray emission. Diffuse emission arising from mechanical feedback would appear extended and resolved. On the other hand, LLAGN should appear as nuclear point sources, so we expect the corresponding X-ray sources to be unresolved. However, a luminous HMXB may also appear as a single ULX, and in more distant galaxies, multiple HMXBs may also appear unresolved; for the most distant object, LARS 12, the $0''.5$ ACIS PSF corresponds to ~ 900 pc.

The source sizes were estimated from the FWHM of axisymmetric radial profiles, using radial annuli large enough to account for pixelization and to cleanly measure the FWHM. The on-axis PSF of *Chandra* ACIS is $0''.5$. For *XMM-Newton* EPIC-pn, MOS-1, and MOS-2, the FWHMs are $12''.5$, $4''.3$, and $4''.4$, respectively.

We find that Haro 11-C, NGC 6090-SW, LARS 01, LARS 12, and possibly LARS 09 are unresolved point sources, corresponding to at least half of the eight LAE sources observed with ACIS. An additional four sources are detected only by XMM, which has much larger PSFs that cannot resolve point sources in these galaxies: ESO 338-IG004, LARS 07, and

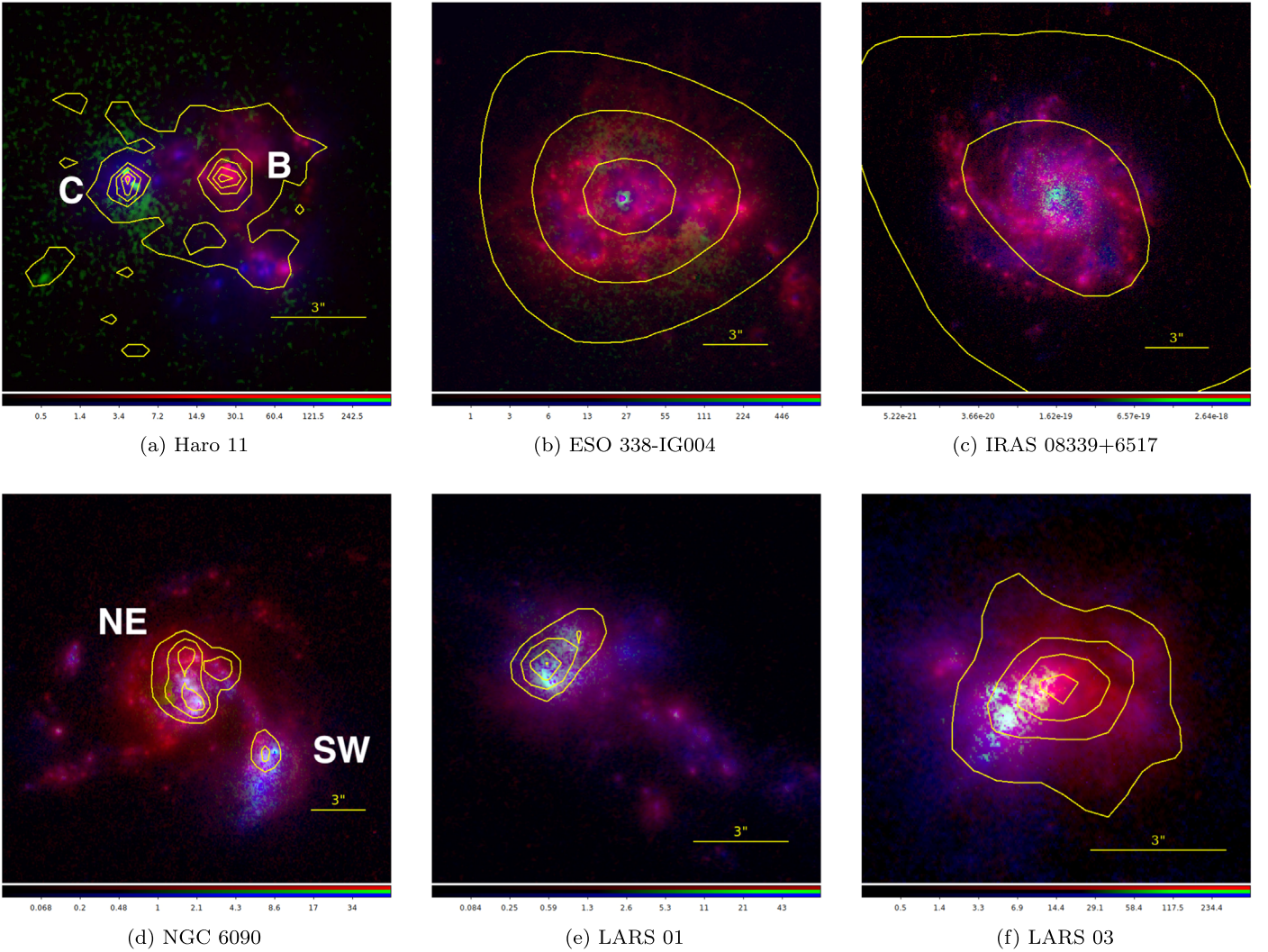


Figure 1. Composite RGB images of galaxies in our sample. $H\alpha$, continuum-subtracted $\text{Ly}\alpha$, and FUV are shown by red, green, and blue, respectively. Contours represent 0.3–10 keV X-ray surface brightness with the significance for each object (in units of σ , where σ is measured from a local background annulus) and Gaussian smoothing kernel in parentheses: Haro 11: 1.7, 15, 28, 42, and 75σ (no smoothing); ESO 338-IG004: 2.0, 6.0, and 11σ (2 pixels); IRAS 08339+6517: 5.9 and 14σ (2 pixels); NGC 6090: 3.9, 5.1, and 5.9σ (2 pixels); LARS 01: 4.0, 6.0, and 8.0σ (3 pixels); LARS 03: 2.8, 4.1, 4.9, and 6.3σ (3 pixels).

LARS 08 are unresolved, and only IRAS 08339+6517 is extended. Overall, 7 of the 12 sources are technically unresolved (boldface in Table 2).

3.2. X-Ray Luminosities

We expect to find HMXBs in these starburst galaxies, since there is a direct, empirical relationship between the total X-ray luminosity L_X from HMXBs, and star formation rate (SFR; Lehmer et al. 2010; Mineo et al. 2012) in star-forming galaxies. This relation also depends on metallicity, so that (Borby et al. 2016)

$$\log L_X / (\text{erg s}^{-1}) = \log \text{SFR} / (M_\odot \text{ yr}^{-1}) + b (12 + \log(\text{O}/\text{H}) - 8.69) + 39.49, \quad (1)$$

where L_X is the luminosity in the 0.5–8 keV band, $b = -0.59 \pm 0.13$ (Borby et al. 2016), and solar metallicity corresponds to $12 + \log(\text{O}/\text{H}) = 8.69$. Low-mass X-ray binaries are not a significant source of X-ray emission in our

starbursts, having orders of magnitude lower total L_X (Mineo et al. 2012).

If L_X is significantly more luminous than expected from this relation, then an LLAGN may be present. In Figure 3, we evaluate this possibility on a statistical basis, calculating L_X from our measured flux values in the 0.5–8.0 keV band. The L_X are in the range $3\text{--}36 \times 10^{40} \text{ erg s}^{-1}$ (Table 2). For the LARS galaxies, we derive the SFR from $H\alpha$ luminosities given by Hayes et al. (2014). For the remaining galaxies, we use the relation from Mineo et al. (2012) that sums the SFRs derived from the NUV and FIR luminosities, using the 2255 Å and FIR fluxes given by Östlin et al. 2009, Table 2).

We find that the LAE galaxies have large $L_X > 10^{40} \text{ erg s}^{-1}$, and generally lie along the L_X –SFR–metallicity relationship (Figure 3). More objects are found above the relation than below. Equation (1) is based on NUV+FIR fluxes (Borby et al. 2016), which tend to overestimate SFR relative to $H\alpha$ (Hirashita et al. 2003); thus there may be a slight systematic offset between the Östlin and LARS subsamples. However, it is the Östlin galaxies that appear to deviate to higher L_X , rather than the LARS galaxies. The already high L_X suggests that soft,

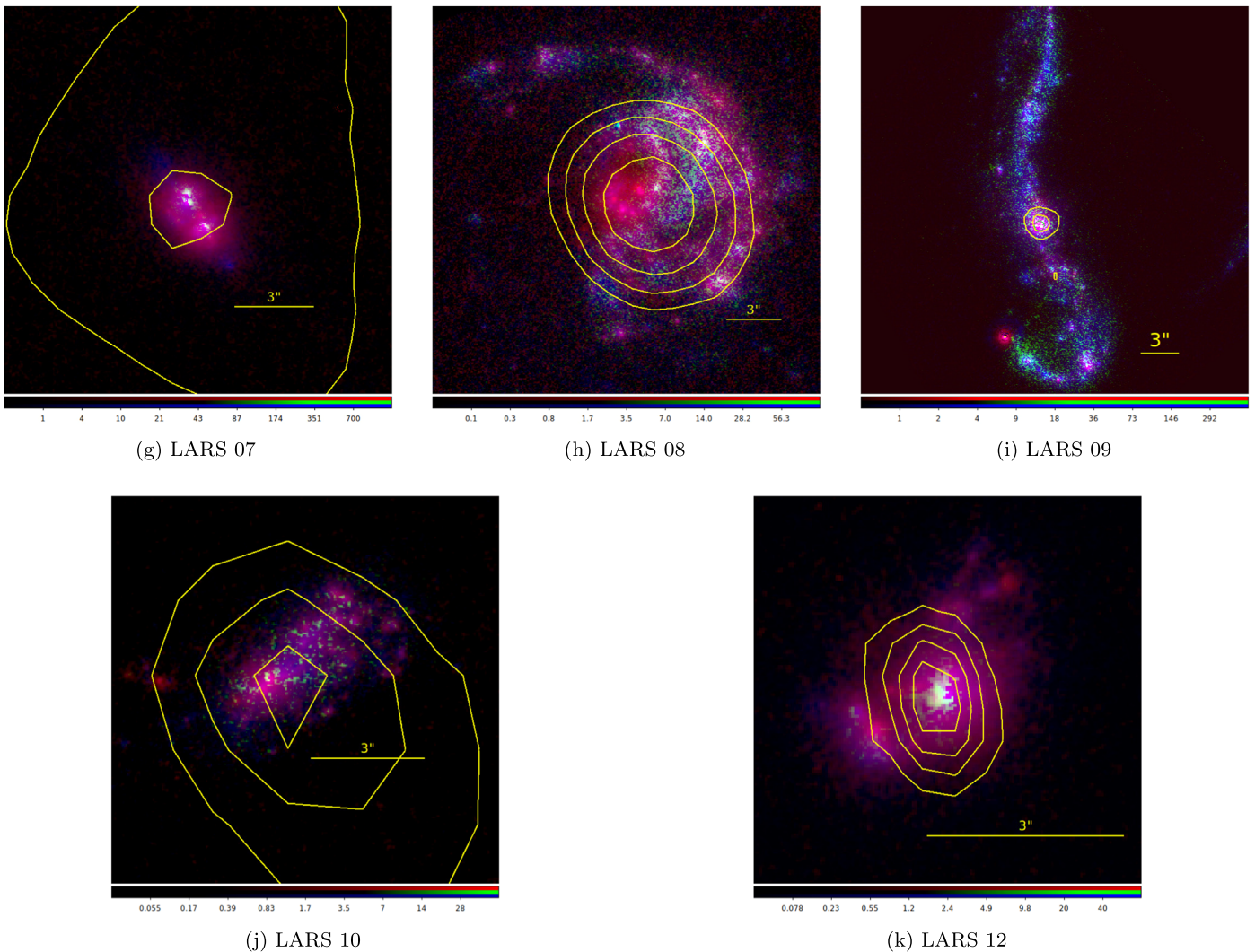


Figure 2. Same as Figure 1, but for the remainder of our sample. LARS 07: 1.5 and 3.1σ (3 pixels); LARS 08: 4.8, 5.8, 6.8, and 7.8σ (3 pixels); LARS 09: 1.8 and 3.5σ (3 pixels); LARS 10: 1.1, 2.2, and 3.2σ (3 pixels); LARS 12: 1.6, 3.3, 5.0, and 6.6σ (3 pixels).

thermal X-ray sources are unlikely to dominate, since such sources would have underestimated values of L_X .

IRAS 08339+6517 has the largest excess L_X (Figure 3). Oti-Floranés et al. (2014) find that its SFR is consistent with their inferred $L_X = 2 \times 10^{41}$ erg s $^{-1}$, which is lower than our result for this galaxy, but the lower L_X would still correspond to a significant excess in Figure 3. Oti-Floranés et al. (2014) estimated the SFR and expected L_X from detailed population synthesis modeling, and so it is hard to compare their conclusion with the empirical L_X -SFR relation. Their analysis may demonstrate the limitations of using this relation for individual galaxies. On the other hand, this galaxy may host an LLAGN candidate.

3.3. Hardness Ratios

We compute hardness ratios (HRs) from the model-independent fluxes measured for each source through CIAO’s `srcflux` function:

$$\text{HR}_{xy} = \frac{F(x) - F(y)}{F(x) + F(y)}, \quad (2)$$

where $F(x)$ and $F(y)$ are the model-independent flux for the hard energy band (2.0–8.0 keV) and soft band (0.5–2.0 keV), respectively. In some cases, the count rates are too low to obtain a useful HR, and we report in Table 2 only values where the HR errors are <0.5 . Figure 3 indicates the hardness ratios by point color. All of the measured HR for our Ly α sources are consistent with $\Gamma = 2.0 \pm 0.5$, which corresponds to $\text{HR} = 0.0 \pm 0.33$. The HR may be significantly overestimated if there is a high H I column; however, the existence of Ly α emission argues against high columns associated with most objects.

We expect LLAGN to show harder states than HMXBs, although there is some variance (e.g., Ho 2008). Interestingly, while the errors are large, there does appear to be a tendency for the objects with excess L_X to have harder HRs in Figure 3.

3.4. Morphology

The morphology of these galaxies provides further insight on the origin of their X-ray emission. We see that spatially resolved observations are essential, since in at least one galaxy, LARS 09, the Ly α and X-ray emission are completely

Table 2
X-Ray Data for Local Ly α -emitting Galaxies

| Name | Instrument | FWHM ^a (arcsec) | f_x (0.5–8 keV) (10^{-14} erg s $^{-1}$ cm $^{-2}$) | L_x (0.5–8 keV) (10^{40} erg s $^{-1}$) | HR | SFR ^b (M_\odot yr $^{-1}$) | Distance ^c (Mpc) | 12 + log(O/H) ^d |
|------------------------------|------------|-------------------------------|--|--|--------------------------|--|--------------------------------|----------------------------|
| Haro 11 | ACIS-S | ... | 21.2 $^{+1.5}_{-1.5}$ | 19.3 $^{+1.4}_{-1.4}$ | ... | 5.15 | 87 \pm 6.1 | 7.9 |
| (Knot B) ^e | ACIS-S | 0.77 | 11.8 $^{+1.1}_{-1.1}$ | 10.7 $^{+1.0}_{-1.0}$ | 0.40 $^{+0.39}_{-0.32}$ | 0.86 | 87 \pm 6 | 8.3 |
| Knot C | ACIS-S | ≤ 0.5 | 7.76 $^{+0.91}_{-0.91}$ | 7.07 $^{+0.83}_{-0.83}$ | ... | 0.09 | 87 \pm 6 | 7.8 |
| NGC 6090 | ACIS-S | ... | 14.2 $^{+1.3}_{-1.3}$ | 28.7 $^{+2.6}_{-2.6}$ | ... | 4.75 | 130 \pm 9 | 8.8 |
| SW Galaxy | ACIS-S | ≤ 0.5 | 2.98 $^{+0.62}_{-0.61}$ | 6.02 $^{+1.25}_{-1.23}$ | ... | 1.57 | 130 \pm 9 | 8.8 |
| NE Galaxy ^g | ACIS-S | 2.4 | 10.4 $^{+1.1}_{-1.1}$ | 21.0 $^{+2.2}_{-2.2}$ | -0.21 $^{+0.18}_{-0.16}$ | 3.18 | 130 \pm 9 | 8.8 |
| IRAS 08339+6517 ^f | EPIC-MOS | 10 | 41.5 $^{+1.7}_{-1.7}$ | 36.5 $^{+1.5}_{-1.5}$ | 0.02 \pm 0.05 | 7.86 | 86 \pm 6 | 8.7 |
| ESO 338-IG004 | EPIC-MOS | 4.5 | 35.8 $^{+1.8}_{-1.8}$ | 6.84 $^{+0.34}_{-0.34}$ | 0.27 \pm 0.05 | 3.90 | 40 \pm 3 | 7.9 |
| LARS 01 | ACIS-S | ≤ 0.5 | 1.96 $^{+0.44}_{-0.43}$ | 3.75 $^{+0.84}_{-0.82}$ | 0.04 $^{+0.39}_{-0.27}$ | 6.52 | 126 \pm 9 | 8.3 |
| LARS 03 | ACIS-S | 1.1 | 15.2 $^{+1.4}_{-1.4}$ | 35.1 $^{+3.2}_{-3.2}$ | 0.33 $^{+0.16}_{-0.11}$ | 26.3 | 139 \pm 10 | 8.4 |
| LARS 07 | EPIC-pn | ≤ 12.5 | 1.00 $^{+0.20}_{-0.20}$ | 3.49 $^{+0.70}_{-0.70}$ | -0.24 \pm 0.25 | 9.27 | 171 \pm 12 | 8.4 |
| LARS 08 | EPIC-pn | ≤ 12.5 | 8.18 $^{+0.50}_{-0.50}$ | 29.3 $^{+1.8}_{-1.8}$ | -0.11 \pm 0.08 | 36.8 | 173 \pm 12 | 8.5 |
| LARS 09 ^g | ACIS-S | 0.57 | 4.86 $^{+1.15}_{-1.15}$ | 25.7 $^{+6.1}_{-6.1}$ | ... | 40.7 | 210 \pm 15 | 8.4 |
| LARS 10 | ACIS-S | 1.5 | 0.41 $^{+0.43}_{-0.28}$ | 3.23 $^{+3.39}_{-2.22}$ | ... | 5.59 | 258 \pm 18 | 8.5 |
| LARS 12 | ACIS-S | ≤ 0.5 | 1.07 $^{+0.45}_{-0.35}$ | 26.4 $^{+11.1}_{-8.6}$ | ... | 97.0 | 454 \pm 32 | 8.4 |

Notes.

^a Instrument PSFs: *XMM* EPIC-pn = 12''5, *XMM* EPIC-MOS = 4''3, *Chandra* ACIS = 0''5. Boldface values are unresolved.

^b SFR based on H α compiled by Hayes et al. (2014) for LARS galaxies, and computed from NUV and FIR fluxes for Östlin et al. (2009) galaxies. For ESO 338-IG004 we adopt 2255 Å flux = 4×10^{-14} erg s $^{-1}$ cm $^{-2}$ Å $^{-1}$ interpolated from adjacent NUV bands in Östlin et al. (2009). Uncertainties are on the order of 0.3 dex or more.

^c Distance from NED.

^d LARS galaxy metallicities compiled by Pardy et al. (2014); remaining objects from Östlin et al. (2009).

^e Haro 11-B is not a significant Ly α source and is included here for comparison.

^f Severely off-axis *XMM* observation; may be unresolved.

^g Multiple X-ray sources. FWHM is measured from the brightest source; other X-ray quantities are integrated over the multiple sources.

unrelated (Figure 2(c)): the X-ray source is in the nucleus, while the Ly α is in the southern outskirts of the galaxy. In Haro 11, the LAE Haro 11-C does not correspond to the dominant X-ray source, Haro 11-B (Figure 1(a); Table 2). The former is a ULX, while the latter could be a faint LLAGN ($L_x = 1.1 \times 10^{41}$ erg s $^{-1}$; Prestwich et al. 2015). Similarly, ESO 338-IG004 has a hard HR, consistent with a candidate LLAGN (Table 2), but Oskinova et al. (2019) recently showed that this is a nonnuclear X-ray source, which is spatially unrelated to the nuclear LAE. They suggest that the object is an intermediate-mass black hole candidate.

For NGC 6090-NE, LARS 03, LARS 08, and LARS 10, the Ly α and X-ray emission are spatially consistent with a physical association but their morphologies do not correlate strongly. Thus, a causal relation between them is ambiguous. Except for LARS 08, these galaxies show extended emission in both X-ray and Ly α , suggesting a possibly important role for luminous star-forming regions and their feedback (Figures 1, 2). LARS 08 has marginal L_x excess, and its Ly α is coincident with nonnuclear UV continuum emission. If the bright, unresolved X-ray source (Figure 2(b)) is however due to an LLAGN candidate, it is likely to be located at the galaxy nucleus, which is heavily obscured by dust (Hayes et al. 2014). Thus, while this galaxy may host an LLAGN, it also does not seem likely to be responsible for the Ly α emission, which is probably due to luminous star-forming regions.

For most of the remaining galaxies, the X-ray emission is consistent, within the astrometric errors, with originating at a nuclear position, or in the case of major mergers, a position consistent with the nucleus of one of the two merging objects. While *XMM* data are spatially unresolved, we note that

all but one of the eight galaxies observed with *Chandra* show nuclear X-ray emission, and in Haro 11-C, NGC 6090-SW, LARS 01, and LARS 12 these nuclear sources are unresolved. Lehmer et al. (2010) suggest that nuclear X-ray emission $L_x > 10^{40}$ erg s $^{-1}$ can usually be attributed to AGN. In any case, our findings suggest that X-ray emission from LAEs is often associated with nuclear activity, whether LLAGN candidates, or nuclear starbursts.

4. Discussion

Our sample of starburst galaxies with spatially resolved Ly α shows that luminous X-ray sources cannot be ruled out as the origin of Ly α emission in 9 of the 12 Ly α sources. In particular, we detect an X-ray source brighter than 10^{40} erg s $^{-1}$ that may be associated with the Ly α emission in each of the 12 Ly α sources, except for LARS 08, LARS 09, and ESO 338-IG004. Of the 9 remaining sources, 7 have *Chandra* observations, and 4 are unresolved X-ray point sources. Extended X-ray emission also does not rule out HMXBs or LLAGN as Ly α sources. Although the selection bias is difficult to evaluate, these results are remarkable, and suggest a significant link between X-rays and observed Ly α .

Extrapolating from L_x down to 13.6 eV yields predicted Ly α luminosities compatible with those observed, for a typical power-law index $\Gamma = 1.5$ –2.0. Our findings are consistent with those of Bluem et al. (2019), who find that five of their eight blue compact galaxies that are Lyman continuum-emitting candidates show significant X-ray excess; and Svoboda et al. (2019) also find X-ray excess in two of their three Green Pea galaxies. As noted in Section 3.2, our sample similarly shows a tendency toward excess L_x .

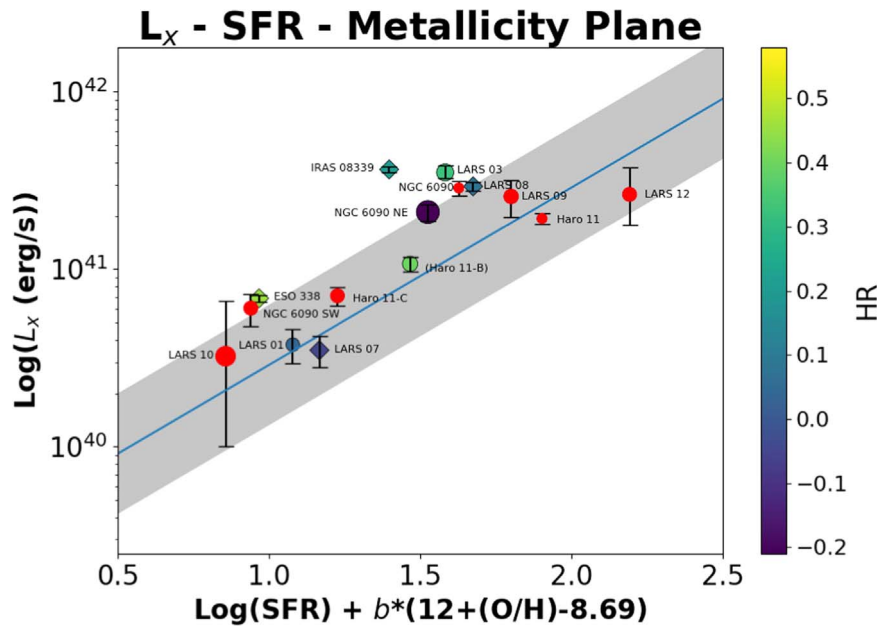


Figure 3. L_X –SFR–metallicity relation for star-forming galaxies, showing our sample and the relation from Brorby et al. (2016; blue line). Their observed 0.34 dex dispersion in the relation is shown by the gray band. Hardness ratio is indicated with the shown color scale; red points indicate objects without enough counts for a reliable HR estimate. Circles show *Chandra* ACIS observations, with point size scaled to source FWHM; diamonds indicate *XMM* data, which cannot resolve point sources in our sample. Haro 11-B is not a significant LAE, but is included for completeness. Data for Haro 11 and NGC 6090 are shown for individual subregions, as well as for total integrated values.

ULXs and/or LLAGN may play an important role in L_{α} emission. IRAS 08339+6517 has significant excess L_X . Also, LARS 03 is elevated in both L_X and HR, although it is extended (Figure 1(f)). These objects are consistent with the recent identification of strong AGN candidates in dwarf galaxies with nebular diagnostics of only star formation (e.g., Reines et al. 2013; Baldassare et al. 2018). And although LLAGN are specifically excluded from Equation (1), galaxies that lie on this relation may still harbor them, e.g., LLAGN candidate Haro 11-B (Prestwich et al. 2015, Figure 3).

Since all of our objects lie on, or above, the L_X –SFR relation, the possible role of HMXBs in driving the LAEs further suggests that compact objects may be a major, and perhaps even dominant, source of L_{α} emission in galaxies. Basu-Zych et al. (2013) also find above-average L_X in their sample of six Lyman-break analog galaxies, which includes two members of our sample. Due to L_{α} scattering properties, feedback and outflows are likely important in allowing L_{α} to escape (e.g., Hayes et al. 2007; Orsi et al. 2012; Wofford et al. 2013). Large numbers of HMXBs form in starbursts after 10–20 Myr, when supernova feedback has had time to clear optically thin pathways, and after ionizing OB stars have expired. Pakull et al. (2010) also show that ULXs in star-forming galaxies can have mechanical feedback that exceeds their X-ray luminosity by orders of magnitude. Similarly, LLAGN could both produce L_{α} and generate escape avenues via disk winds and jet feedback.

The possible role of HMXBs and LLAGN in powering L_{α} sources implies that LAEs may be much longer lived than massive stars in the parent starbursts. HMXBs dominate populations at ages of 10–20 Myr, and low-level accretion in an LLAGN can be sustained on timescales $10\times$ longer or more. This has far-reaching implications for interpreting L_{α} observations and understanding cosmic reionization. We also note that the possible presence of LLAGN in many star-forming

galaxies could also affect calibration of the L_X –SFR relation. Moreover, HMXBs are believed to be responsible for an earlier era of cosmic heating preceding reionization (Fragos et al. 2013), to be detected with new-generation 21-cm surveys. If LLAGN are confirmed in our sample, it would not necessarily affect the impact of HMXBs on cosmic dawn, but rather highlights the need to clarify the relative contributions of LLAGN, HMXBs, and stellar photoionization to the production of L_{α} over cosmic time (Lehmer et al. 2016).

We thank the anonymous referee for helpful comments. This work was supported in part by NASA grant 80NSSC18K0376 to E.H.K. and HST-GO-15352.002-A to M.S.O. M.H. and G.O. acknowledge the support of the Swedish Research Council, Vetenskapsrådet and the Swedish National Space Agency (SNSA). M.H. is a Fellow of the Knut and Alice Wallenberg Foundation.

ORCID iDs

M. S. Oey <https://orcid.org/0000-0002-5808-1320>

Edmund Hodges-Kluck <https://orcid.org/0000-0002-2397-206X>

Matthew Hayes <https://orcid.org/0000-0001-8587-218X>

Jens Melinder <https://orcid.org/0000-0003-0470-8754>

References

- Baldassare, V. F., Geha, M., & Greene, J. 2018, *ApJ*, **868**, 152
 Basu-Zych, A. R., Lehmer, B. D., Hornschemeier, A. E., et al. 2013, *ApJ*, **774**, 152
 Bluem, J., Kaaret, P., Prestwich, A., & Brorby, M. 2019, *MNRAS*, **487**, 4093
 Brorby, M., Kaaret, P., Prestwich, A., & Mirabel, I. F. 2016, *MNRAS*, **457**, 4081
 Calhau, J., Sobral, D., Santos, S., et al. 2020, *MNRAS*, submitted (arXiv:1909.11672)
 Fragos, T., Lehmer, B. D., Naoz, S., Zezas, A., & Basu-Zych, A. 2013, *ApJL*, **776**, L31

- Hashimoto, T., Garel, T., Guiderdoni, B., et al. 2017, *A&A*, 608, A10
- Hayes, M., Östlin, G., Atek, H., et al. 2007, *MNRAS*, 382, 1465
- Hayes, M., Östlin, G., Duval, F., et al. 2014, *ApJ*, 782, 6
- Herenz, E. C., Wisotzki, L., Saust, R., et al. 2019, *A&A*, 621, A107
- Hirashita, H., Buat, V., & Inoue, A. K. 2003, *A&A*, 410, 83
- Ho, L. C. 2008, *ARA&A*, 46, 475
- Hu, E. M., & McMahon, R. G. 1996, *Natur*, 382, 231
- Kashikawa, N., Shimasaku, K., Malkan, M. A., et al. 2006, *ApJ*, 648, 7
- Lehmer, B. D., Alexander, D. M., Bauer, F. E., et al. 2010, *ApJ*, 724, 559
- Lehmer, B. D., Basu-Zych, A. R., Mineo, S., et al. 2016, *ApJ*, 825, 7
- Malhotra, S., & Rhoads, J. E. 2004, *ApJL*, 617, L5
- Mallery, R. P., Mobasher, B., Capak, P., et al. 2012, *ApJ*, 760, 128
- Mineo, S., Gilfanov, M., & Sunyaev, R. 2012, *MNRAS*, 419, 2095
- Orsi, A., Lacey, C. G., & Baugh, C. M. 2012, *MNRAS*, 425, 87
- Oskina, L. M., Bik, A., Mas-Hesse, J. M., et al. 2019, *A&A*, 627, A63
- Östlin, G., Hayes, M., Duval, F., et al. 2014, *ApJ*, 797, 11
- Östlin, G., Hayes, M., Kunth, D., et al. 2009, *AJ*, 138, 923
- Otí-Flóranes, H., Mas-Hesse, J. M., Jiménez-Bailón, E., et al. 2014, *A&A*, 566, A38
- Pakull, M. W., Soria, R., & Motch, C. 2010, *Natur*, 466, 209
- Pardy, S. A., Cannon, J. M., Östlin, G., et al. 2014, *ApJ*, 794, 101
- Partridge, R. B., & Peebles, P. J. E. 1967, *ApJ*, 148, 377
- Prestwich, A. H., Jackson, F., Kaaret, P., et al. 2015, *ApJ*, 812, 166
- Reines, A. E., Greene, J. E., & Geha, M. 2013, *ApJ*, 775, 116
- Sazonov, S., & Khabibullin, I. 2017, *MNRAS*, 466, 1019
- Stark, D. P., Ellis, R. S., Charlot, S., et al. 2017, *MNRAS*, 464, 469
- Svoboda, J., Douma, V., Orlitová, I., & Ehle, M. 2019, *ApJ*, 880, 144
- Terashima, Y., Iyomoto, N., Ho, L. C., & Ptak, A. F. 2002, *ApJS*, 139, 1
- Wofford, A., Leitherer, C., & Salzer, J. 2013, *ApJ*, 765, 118